The relative formation ages of ferromagnesian chondrules inferred from their initial aluminum-26/aluminum-27 ratios

SMAIL MOSTEFAOUI[1,3]*, NORIKO T. KITA[1], SHIGEKO TOGASHI[1], SHOGO TACHIBANA[2†], HIROKO NAGAHARA[2] AND YUICHI MORISHITA[1]

[1]Geological Survey of Japan, AIST, AIST Central-7, Tsukuba 305-8567, Japan
[2]Department of Earth and Planetary Science, University of Tokyo, Hongo, Tokyo 113-0033, Japan
[3]Max Planck Institute for Chemistry, Cosmochemistry Department, J. J. Becher-Weg 27, D-55020 Mainz, Germany
[†]Present address: Department of Geological Sciences, Arizona State University, Tempe, Arizona 85287-1404, USA
*Correspondence author's e-mail address: smail@mpch-mainz.mpg.de

Abstract–We performed a systematic high-precision secondary ion mass spectrometry ^{26}Al-^{26}Mg isotopic study for 11 ferromagnesian chondrules from the highly unequilibrated ordinary chondrite Bishunpur (LL3.1). The chondrules are porphyritic and contain various amounts of olivine and pyroxene and interstitial plagioclase and/or glass. The chemical compositions of the chondrules vary from FeO-poor to FeO-rich. Eight chondrules show resolvable ^{26}Mg excesses with a maximum δ^{26}Mg of ~1% in two chondrules. The initial ^{26}Al/^{27}Al ratios inferred for these chondrules range between $(2.28 \pm 0.73) \times 10^{-5}$ to $(0.45 \pm 0.21) \times 10^{-5}$. Assuming a homogeneous distribution of Al isotopes in the early solar system, this range corresponds to ages relative to CAIs between 0.7 ± 0.2 Ma and $2.4^{-0.4}_{+0.7}$ Ma. The inferred total span of the chondrule formation ages is at least 1 Ma, which is too long to form chondrules by the X-wind. The initial ^{26}Al/^{27}Al ratios of the chondrules are found to correlate with the proportion of olivine to pyroxene suggesting that olivine-rich chondrules formed earlier than pyroxene-rich chondrules. Though we do not have a completely satisfactory explanation of this correlation we tentatively interpret it as a result of evaporative loss of Si from earlier generations of chondrules followed by addition of Si to the precursors of later generation chondrules.

INTRODUCTION

One of the most extensively debated subjects in meteoritics is the origin of chondrules, their heating mechanisms, and the timescales of their formation. The relative chronometer based on the decay of the extinct radionuclide ^{26}Al (which decays to ^{26}Mg with a half-life of 0.73 Ma), applied to individual chondrules, is an outstanding tool to determine the timing of chondrule formation relative to calcium-aluminum-inclusion (CAI) formation (*e.g.*, Hutcheon and Jones, 1995; Russell *et al.*, 1996; Kita *et al.*, 2000). Previous studies on both Al-rich and ferromagnesian chondrules in unequilibrated ordinary chondrites showed that chondrule formation events started ~2 Ma after CAIs formed (Hutcheon and Hutchison, 1989; Russell *et al.*, 1996; Kita *et al.*, 2000; Huss *et al.*, 2001). It is not clear if the duration of chondrule formation events was as short as 1 Ma (Kita *et al.*, 2000) or extended to more than 5 Ma (Russell *et al.*, 1996). Considering that all younger ages were obtained from chondrules of type 3.4 ordinary chondrites, it is likely that the Al-Mg system in these chondrules was disturbed by parent-body metamorphism. Therefore, in order to study

chondrule formation ages unambiguously, investigation of chondrule Al-Mg ages should be limited to highly unequilibrated chondrites (Kita *et al.*, 2000).

Most of the previous chondrule Al-Mg data were obtained from Al-rich chondrules because they contain phases with high Al/Mg ratios suitable for the analysis. However, Al-rich chondrules are rare and accordingly do not represent the total chondrule population. The most representative are ferromagnesian chondrules, which constitute more than 80% of the total chondrule population (Gooding and Keil, 1981). The problem for ferromagnesian chondrules, however, is that they generally consist of phases with low Al/Mg ratios making it difficult for any radiogenic ^{26}Mg to be detected. Using the high-sensitivity and high-resolution secondary ion mass spectrometer (SIMS) (IMS-1270 at the Geological Survey of Japan), Kita *et al.* (2000) performed a high-precision Mg isotopic analysis with a 3–5 μm spot size. For Semarkona ferromagnesian chondrules, ^{26}Mg excesses were detected in all chondrules in interstitial glass and plagioclase with high Al/Mg ratios. The initial ^{26}Al/^{27}Al ratios of the Semarkona chondrules are $(0.4–0.9) \times 10^{-5}$, corresponding to their formation ~2 Ma after CAIs. Similar

results were recently obtained for several ferromagnesian chondrules in Semarkona and Bishunpur (McKeegan *et al.*, 2000) and Al-rich chondrules in carbonaceous chondrites (Hutcheon *et al.*, 2000; Srinivasan *et al.*, 2000a,b).

In this work we present data from 11 ferromagnesian chondrules in the Bishunpur chondrite. Bishunpur is one of the most primitive chondrites and much work has been performed on its constituents in order to understand the early evolution of solar system materials (*e.g.*, Rambaldi and Wasson, 1981; Mostefaoui *et al.*, 2000). The disturbance of the Al-Mg system during parent-body processes is assumed to be minimal for this meteorite. In an early stage of this study, we analyzed a few chondrules with various amounts of olivine and pyroxene. When we combined these results with those of five chondrules from Semarkona previously studied by Kita *et al.* (2000), we noticed that pyroxene-rich chondrules tend to show lower initial $^{26}Al/^{27}Al$ ratios. For this reason, we decided to study chondrules with a wide range of olivine and pyroxene proportions and to pay special attention to the olivine-pyroxene proportions of the analyzed chondrules. Here, we present a high-resolution age determination of ferromagnesian chondrules and report for the first time a systematic age difference between olivine-rich and pyroxene-rich chondrule end members.

ANALYTICAL TECHNIQUES

Selection of Chondrules for the Aluminum-Magnesium Measurements

We examined ferromagnesian chondrules in two polished thin sections of Bishunpur (hereafter refered to as section B1 and B2, which are "M3816" from the Natural History Museum, Vienna, and "05-DE" from the Natural History Museum, London, respectively). Petrographic observation and chemical analyses of individual samples were carried out using an optical microscope and an electron microprobe. Quantitative analyses of major elements in minerals and glasses were performed using an electron microprobe (EPMA; JEOL JXA-8800R Super-probe) at an accelerating voltage of 15 keV, a beam diameter of 2 μm, and a beam current of 12 nA for minerals and 3 nA for glasses. The counting time was set to 20 s for both mineral and glass analyses. The data were reduced with the Bence and Albee correction method.

We selected chondrules that had phases with Al/Mg ratios high enough for detecting radiogenic ^{26}Mg using SIMS. Phases with $Al_2O_3/MgO > 50$ are suitable candidates. The entire areas of the two Bishunpur polished sections (Fig. 1) were carefully examined for Al-rich phases in chondrules. Among 70 chondrules in section B1 and 24 in section B2, we only found 11 chondrules (~12% of the studied chondrules) suitable for SIMS measurements. The Al-rich phases in the chondrules (identified as plagioclase and/or glass) were then located and photographed. Because of the analytical requirement to measure high Al/Mg phases, selection of samples might be biased to relatively rare types of chondrules. However, 11 chondrules studied here also contain many typical type I and type II chondrules, and covering a wide range of compositional and textural varieties.

In order to observe the spatial distribution of olivine, pyroxene and aluminous phases in the chondrules, we made EPMA x-ray maps of eight major elements (Na, Mg, Al, Si, S, Ca, Fe, and Ni). This procedure was useful to locate olivine and pyroxene in the chondrules in order to determine their spatial distribution and to estimate their relative proportions. X-ray maps of five Semarkona chondrules studied by Kita *et al.* (2000) were also obtained. An accurate estimate of the olivine to pyroxene ratio in each chondrule was done by treating the x-ray maps using computer graphics software.

Secondary Ion Mass Spectrometry Analysis

The Cameca IMS-1270 at the Geological Survey of Japan was used for the ^{26}Al-^{26}Mg isotopic measurements of plagioclase and glass according to the procedure given by Kita *et al.* (2000). A primary ion beam of O_2^- was shaped to a diameter of ~5 μm with an ion intensity of ~33 pA. In order to avoid high Mg ion intensity from the surrounding Mg-silicates, we carefully selected clean and inclusion-free areas and observed Al and Mg ion images before each analysis.

Three plagioclase (An_{95}-An_{60}) and four glass (basalt, andesite, and rhyolite) standards are used to calibrate the SIMS $^{27}Al/^{24}Mg$ ratios. The relative sensitivity factors, defined as $F = (^{27}Al/^{24}Mg)_{SIMS}/(^{27}Al/^{24}Mg)_{true}$, are estimated for plagioclase and glass standards. The reproducibility of these standards was 10% (2σ), which should be considered the uncertainty of a single analysis. As shown in Table 1, the values of *F* for individual standards do not change significantly over the period of nearly 1 year. The *F* values of glass standards ($F \approx 0.9$) showed only a small variation (3%) despite the large variation in the major element compositions. The *F* values of the An_{95} plagioclase standards (~1.3) are systematically higher than that of the An_{60} plagioclase standard (~1.15). Decreasing of *F* values with decreasing anorthite contents was also observed for An_{95}-An_{20} plagioclase standards during trace element analyses in our SIMS laboratory (Kita, unpubl. data). By extrapolating these data linearly to albitic compositions we used *F* values of 1.25 and 1.0 for anorthitic ($An_{>80}$) and albitic ($An_{<30}$) plagioclase compositions, respectively. The *F* value for albitic plagioclase is close to those of glass standards.

After every analysis session, we checked the positions of the SIMS spots, and if necessary, we took photographs and compared them to those obtained before analysis. Using this inspection routine, measurements taken on holes, cracks, mixtures of more than one phase, or irregular surfaces that can give fractionated data were rejected from the data set.
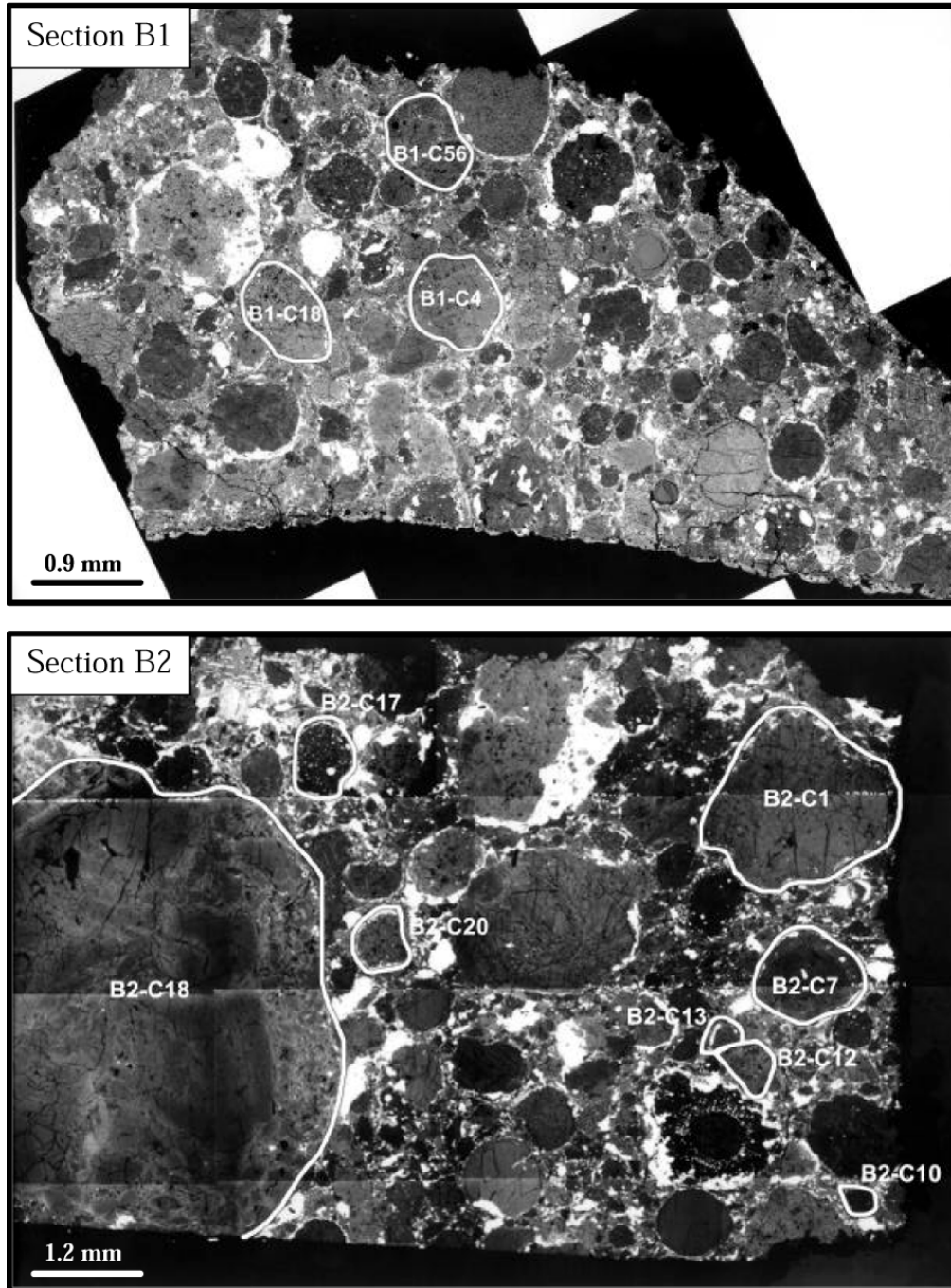
FIG. 1. Mosaics of backscattered electron images for the two Bishunpur thin sections studied: B1(#M3816) and B2 (#05-DE). Among 24 and 79 chondrules in B1 and B2, respectively, only 3 and 8 chondrules (indicated in the figure) have high Al/Mg phases suitable for Mg-isotopic analysis using SIMS.

RESULTS

Petrography

The 11 chondrules we studied are porphyritic with the main constituent minerals being olivine and pyroxene. Textures varied from microporphyritic to coarse porphyritic (Fig. 2).

They have variable sizes ranging from 330×250 μm^2 for B2-C13 to 5270×5160 μm^2 for B2-C18 (an exceptionally large chondrule). Their shapes are essentially spherical, except for B2-C12 and B2-C13, which have irregular boundaries. The irregular boundaries indicate that they could be fragments from larger chondrules. According to the compositions of olivine and pyroxene (see Tables 2 and 3), two chondrules are type I

TABLE 1. Plagioclase mineral standards and geological glass standards used for SIMS analyses.*

Standards	Phase	Al_2O_3 (wt%)	MgO (wt%)	$^{27}Al/^{24}Mg$	F (relative sensitivity factor)[†]		
					99-April	99-June	99-November
AN	An_{95}	35.5	0.083	428	–	1.29	1.31
HACHIJO	An_{95}	35.6	0.110	323	–	1.30	1.32
LAB1	An_{60}	29.4	0.132	223	–	1.15	1.18
ATHO-G	Rhyolite glass	11.79	0.088	134	–	–	0.86
StHs6-80	Andesite glass	17.60	1.97	8.95	–	–	0.91
T1G	Basalt glass	17.04	3.73	4.57	–	–	0.89
JB1a-glass	Basalt glass	14.45	7.83	1.85	0.86	0.85	0.88
Average glass standards	–	–	–	–	–	–	0.89
Dead time (in nanoseconds)	–	–	–	–	31	43	33

*The Al_2O_3 wt% and MgO wt% contents of plagioclase were determined using inductively-coupled plasma mass spectrometry for MgO and EPMA for Al_2O_3, those of the geological glass standards issued by Max Planck Institute are from Jochum *et al.* (2000) and those of JB1a-glass are from the recommended value of the original reference standard (Imai *et al.*, 1995).
[†]The definition is given in the text. Reproducibility of F during the same analytical session is 10% (2σ).

(one IAB and one IB) and the others are type II (seven type IIAB and two IIB).

Mg x-ray maps were used to identify olivine and pyroxene (Fig. 3). In most cases, olivine grains are enclosed in pyroxene; pyroxene is seldom observed inside olivine (*e.g.*, chondrule B2-C17; Fig. 3e). In some olivine-bearing chondrules, pyroxene grains are localized in the outer parts of the chondrules (B1-C18, B2-C1, B2-C10).

Among the chondrules we studied, B2-C18 is exceptionally large and olivine grains show spherical outlined shapes suggesting that they may be the surface of a former chondrule. In this case, the olivine grains could be relics from a previous generation of chondrules.

The Mg maps were also used to determine an estimate of the pyroxene to olivine ratio in the chondrules. For this purpose we calculated the areas of pyroxene and olivine using a computer graphics software. Our results, shown in Table 2, indicate that the proportion of pyroxene, defined as $px = $ [pyroxene]/[olivine + pyroxene], varies from ~22 to 100%. Therefore, the Bishunpur chondrules we examined sample a significant variety of the ferromagnesian types (*i.e.*, from porphyritic olivine-pyroxene (POP) to porphyritic pyroxene (PP)). In this calculation, the error for px is caused by the numbers of pixels counted from the x-ray maps and is normally <10%. Although the px is estimated precisely for the specific cross-sectional view of each chondrule, this estimate represents the relative amounts of pyroxene and olivine and not the pyroxene modal composition because pyroxene and olivine are not the sole phases in chondrules. For this reason, we do not assign errors to px values for the chondrules.

Chemistry of Individual Chondrules

The results of our EPMA analyses of glasses and minerals in chondrules are summarized in Tables 2 and 3. Compositions of the silicate minerals and glasses are variable from chondrule to chondrule, but are relatively uniform within individual chondrules. The molar MgO/(MgO + FeO)% (hereafter referred to as *mg#*) of olivine and low-Ca pyroxene phenocrysts ranges between 77 and 99.5. Strong compositional zoning is observed for olivine in B2-C7 and B2-C20. Some olivine grains in B2-C7 have cores of significantly forsteritic compositions (maximum Fo_{94}), but since low-Ca pyroxene and many other olivine grains in this chondrule have *mg#* of <90 we classified it as a type II. The calculated *mg#* of pyroxene phenocrysts in B2-C13 ranges between 91 and 90, which is at the lower end of type I composition. However, additional EPMA analyses of the same chondrule (Tachibana *et al.*, 2001) showed that the *mg#* of pyroxene extends down to 87. We accordingly classified B2-C13 as type II. In B2-C20, one pyroxene grain has a distinctly higher enstatite content (En_{94}) and much lower CaO and FeO than the rest of the pyroxene grains, suggesting the former is probably a relic. B2-C12 shows strongly zoned pyroxene, which is typical for type II POP chondrules. In this chondrule, one grain is nearly pure forsteritic olivine that may be also a relic. Ca-pyroxene is found in most of the chondrules, as rims around low-Ca pyroxene or as small (less than a few microns) and abundant micro-crystallites in the mesostasis. Analyses of some of the Ca-pyroxene grains showed that they range from $Wo_{15}En_{31}$ to $Wo_{36}En_{52}$.

The Al-rich phases in the chondrules are plagioclase and/or glass (Fig. 4, Table 2). They constitute the interstitial mesostasis to the olivine and pyroxene. As noted above, significant amounts of Ca-pyroxene micro-crystallites are often present in the mesostasis. Plagioclase is present in seven chondrules and has, in most cases, anorthitic composition (An_{80} to An_{93}). Two chondrules contain albitic plagioclase (An_{5-34} in B1-C56 and An_{20} in B2-C17). Plagioclase coexists with glass in three chondrules (two of them are type I). The four other chondrules contain glass but no plagioclase. The glasses in
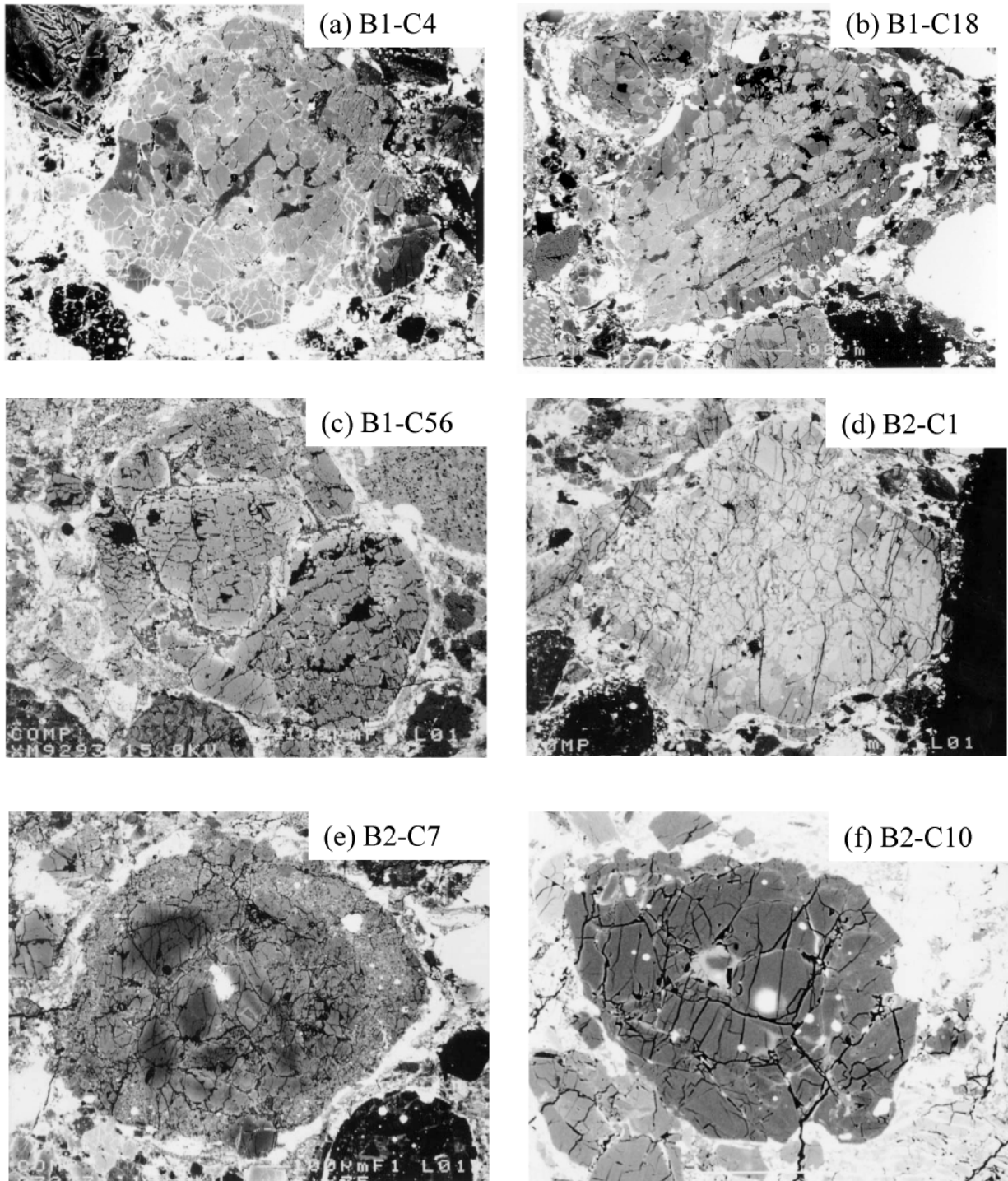
FIG. 2. Backscattered electron images of the 11 chondrules studied with SIMS. All chondrules are porphyritic. (a) B1-C4 (IIAB) contains predominantly coarse olivine crystals (light grey) with minor pyroxene. Anorthitic plagioclase (An_{90}; dark) is present in the center, filling the spaces between the olivine crystals. (b) B1-C18 (IIAB) consists of coarse elongated laths of olivine (light gray) and pyroxene (dark). Most of the pyroxene grains are located in the outer part of the chondrule. Plagioclase is minor and anorthitic (~An_{90}). (c) B1-C56 (IIB) consists predominantly of large pyroxene crystals and has heterogeneous silicate compositions (see Table 2). A large unzoned pyroxene crystal (the one having a triangular shape, possibly a relic grain) is visible in the center surrounded by plagioclase, small olivine, and Ca-pyroxene grains. (d) B2-C1 (IIAB) is olivine-rich, and pyroxene is only present in the outer parts of the chondrule. Plagioclase crystals (An_{87}) are interstitial to the olivine. (e) B2-C7 (IIAB) has a core consisting of coarse olivine, relatively smaller pyroxene phenocrysts, and interstitial glassy mesostasis, surrounded by a fine-grained rim (~100 μm thick) of olivine and pyroxene crystals. (f) B2-C10 (IAB) consists mostly of olivine. Pyroxene is present only in the outer parts of the chondrule. Al-rich glass (light gray area in the center) is the only Al-rich phase found in this chondrule. Small metal grains are visible in olivine. *Figure 2 is continued on the next page.*
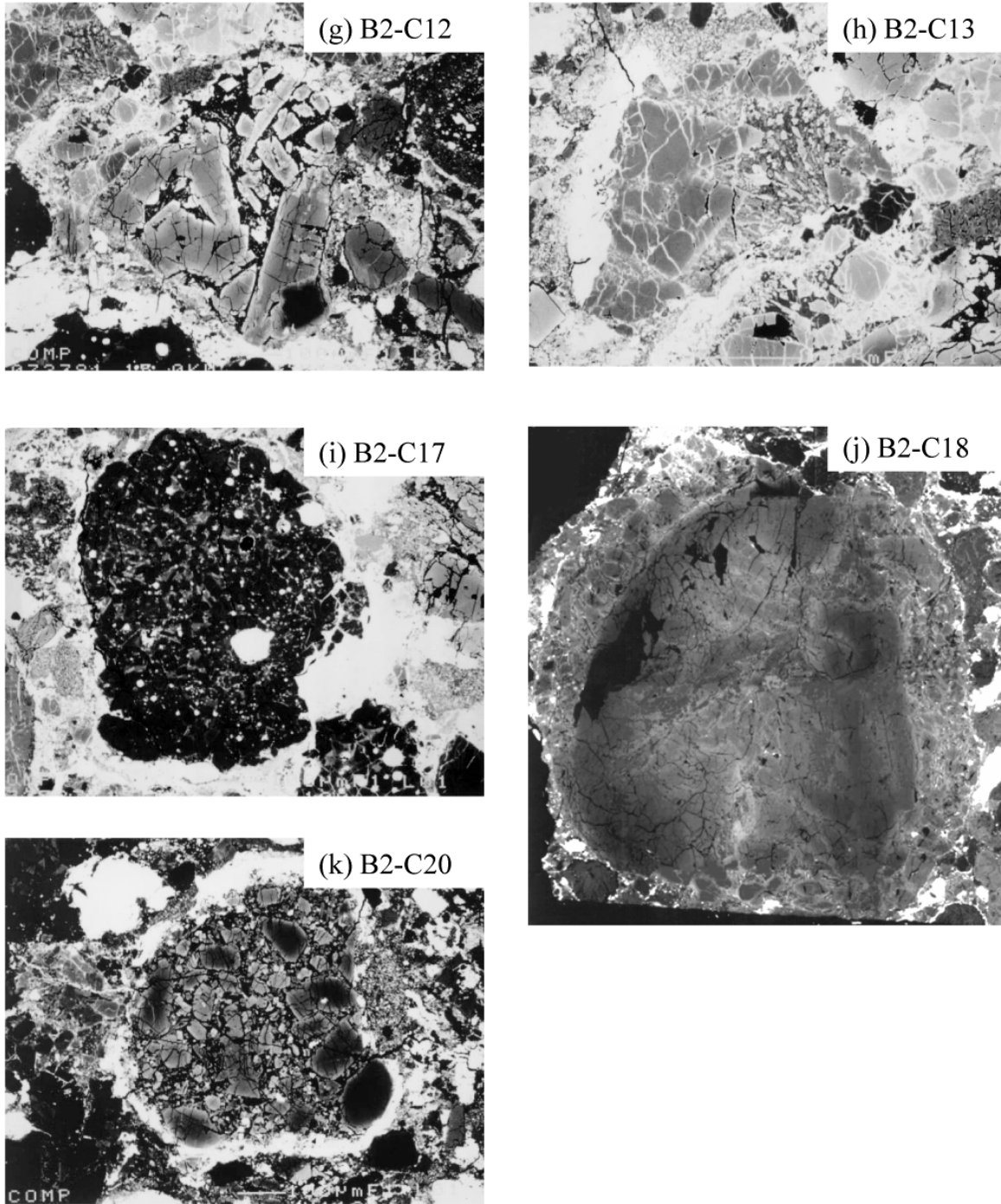
FIG. 2. *Continued.* Backscattered electron images of the 11 chondrules studied with SIMS. All chondrules are porphyritic. (g) B2-C12 (IIAB) shows zoned olivine and pyroxene crystals. A forsteritic olivine grain (dark area below) which is partly surrounded by pyroxene phenocryst may be a relic grain. Interstitial glass is abundant in the chondrule and contains Ca-pyroxene microcrystallites. Smaller olivine and pyroxene phenocrysts are more FeO-rich than the larger phenocrysts. The boundary of the chondrule is not very well defined but the outline shows that the chondrule is not completely circular. (h) B2-C13 (IIB) may be a chondrule fragment with zoned pyroxene. Both plagioclase ($\sim An_{80}$) and glass are present and co-exist with Ca-pyroxene. Olivine is absent in this chondrule. (i) B2-17 (IB) consists predominantly of pyroxene, with minor olivine grains poikilitically enclosed in it, and metal spherules (bright areas). Interstitial glass and rare albitic plagiocalse ($\sim An_{20}$) are also present in the chondrule. (j) B2-C18 (IIAB) is a large chondrule (5 mm in diameter), consisting of a core of large olivine and pyroxene phenocrysts and a rim (700 μm thick) of smaller pyroxene phenocrysts. Zoning features are found in various grains in different parts of the chondrule. The messostasis consists of plagioclase ($\sim An_{90}$) and glass associated with Ca-pyroxene. (k) B2-C20 (IIAB) consists mostly of porphyritic to microporphyritic olivine, pyroxene with smaller grain sizes, and minor interstitial glass. Most of the olivine and pyroxene grains are significantly zoned.

TABLE 2. Ferromagnesian chondrules analyzed for the ^{26}Al-^{26}Mg study.

Chondrule	Type	Size (μm²)	px* (%)	mg#† Olivine	mg#† Low Ca-pyroxene	Aluminous phase	Na₂O % in glass	Reference
Bishunpur								
B1-C4	IIAB	940 × 850	22	83–84	85	An₈₈₋₉₂	–	This work
B1-C18	IIAB	1060 × 750	43	76–78	78–80	An₈₈₋₉₃	–	This work
B1-C56	IIB	750 × 560	87	50, 80	83–88	An₅₋₃₄	–	This work
B2-C1	IIAB	2030 × 1830	24	80–83	84–86	An₈₃₋₉₁	–	This work
B2-C7	IIAB	1260 × 1030	52	84–94	88–89	Al, Si-rich glass	0.3–6	This work
B2-C10	IAB	400 × 300	26	98–99.5	99	Al, Si-rich glass	2–4	This work
B2-C12	IIAB	600 × 500	56	83–86, 99.5	70–83	Al, Si-rich glass	7–10	This work
B2-C13	IIB	330 × 250	100	none	91–92	An₈₀₋₈₄ and basaltic glass	2	This work
B2-C17	IB	770 × 630	95	95	96–98	An₂₀ and Al, Si-rich glass	2.5–10	This work
B2-C18	IIAB	5270 × 5160	46	78	71–81	An₈₆₋₉₀ and basaltic glass	2–8	This work
B2-C20	IIAB	600 × 530	30	76–88	78, 94	Al, Si-rich glass	1–1.5	This work
Semarkona								
1805-9 CH3	IAB	800 × 800	65	97	97	An₉₉.₇	–	(1), this work
1805-9 CH4	IIAB	1100 × 600	40	84–80	81	Al, Si-rich glass	2–8	(1), this work
1805-9 CH23	IIAB	1600 × 1200	29	82	81–84	An₉₉.₇	–	(1), this work
1805-9 CH36	IIAB	1400 × 1000	55	76	77	Al, Si-rich glass	2–8	(1), this work
1805-9 CH60	IIB	700 × 300	83	85	85–88	An₃₄ and Al, Si-rich glass	–	(1), this work
1805-CC1	IIAB	–	37	–	–	Anorthite	–	(2)

*px = [pyroxene]/[olivine + pyroxene] ratio as defined in the text.
†$mg\#$ is the molar MgO/(MgO + FeO)%.
B1 and B2 refer to the two thin sections of Bishunpur. Chondrule types are after Jones (1994). Details of the EPMA analytical results of Bishunpur chondrules are shown in Table 3. Data for Semarkona are from (1) Kita et al. (2000) and (2) Hutcheon and Hutchison (1989). Pyroxene (vol%) of Semarkona 1805-9 chondrules are obtained in this study.

TABLE 3. Electron microprobe analyses of Bishunpur chondrules.*

Chondrule/phase	Nr	SiO_2	TiO_2	Al_2O_3	Cr_2O_3	FeO	MnO	MgO	CaO	Na_2O	K_2O	Total	Composition
B1-C4 (IIAB)													
Olivine	2	38.44	0.03	0.03	0.42	15.66	0.23	44.63	0.20	0.01	0.01	99.62	Fa_{83-84}
Pyroxene	10	54.72	0.00	1.83	1.25	9.42	0.16	30.44	1.60	0.04	0.02	99.48	$En_{81-84}Fs_{13-16}Wo_{3-4}$
Plagioclase	6	45.89	0.02	33.88	0.02	0.66	0.01	0.65	18.26	1.09	0.01	100.48	An_{88-92}
B1-C18 (IIAB)													
Olivine	8	38.83	0.00	0.05	0.12	21.07	0.35	39.81	0.22	0.02	0.01	100.47	Fa_{75-79}
Pyroxene	7	54.53	0.00	1.30	1.01	11.78	0.41	28.10	2.34	0.05	0.01	99.54	$En_{73-79}Fs_{18-19}Wo_{3-8}$
Ca-pyroxene	2	51.16	0.00	2.59	0.96	10.13	0.33	20.85	12.07	0.10	0.02	98.21	$En_{57-61}Fs_{14-18}Wo_{21-29}$
Plagioclase	9	46.05	0.03	33.81	0.02	0.96	0.02	0.60	18.43	1.04	0.00	100.97	An_{88-93}
B1-C56 (IIB)													
Olivine	3	37.64	0.01	0.01	0.09	26.20	1.25	35.81	0.26	0.02	0.01	101.30	Fo_{50-81}
Pyroxene	11	56.56	0.05	0.37	0.82	9.81	0.60	31.64	0.86	0.01	0.01	100.72	$En_{68-88}Fs_{12-22}Wo_{0-10}$
Ca-pyroxene	1	52.39	0.39	2.55	1.52	9.06	1.13	17.88	14.70	0.31	0.00	99.94	$En_{53}Fs_{15}Wo_{32}$
Plagioclase	9	63.11	0.12	23.44	0.01	0.44	0.01	0.13	4.47	8.76	0.02	100.52	An_{3-35}
B2-C1 (IIAB)													
Olivine	15	38.64	0.03	0.02	0.32	17.43	0.25	42.87	0.21	0.02	0.01	99.82	Fo_{80-83}
Pyroxene	9	54.77	0.13	1.70	1.30	10.05	0.21	30.52	1.49	0.03	0.01	100.22	$En_{80-84}Fs_{14-16}Wo_{2-4}$
Plagioclase	4	46.77	0.02	32.71	0.01	0.90	0.01	0.76	16.97	1.44	0.01	99.60	An_{83-81}
B2-C7 (IIAB)													
Olivine	28	40.17	0.02	0.01	0.34	9.73	0.37	48.76	0.10	0.02	0.01	99.54	Fo_{84-94}
Pyroxene	3	55.97	0.05	0.31	0.97	7.80	0.61	31.63	1.24	0.08	0.00	98.67	$En_{84-89}Fs_{10-13}Wo_{1-4}$
Glass	8	71.34	–	15.33	0.27	3.32	0.18	1.94	2.13	4.95	1.16	100.62	–
B2-C10 (IAB)													
Olivine	7	41.49	0.05	0.18	0.19	0.77	0.04	56.44	0.38	0.02	0.01	99.57	$Fo_{98-99.5}$
Pyroxene	5	58.14	0.18	0.99	0.39	0.60	0.07	38.60	0.47	0.04	0.00	99.48	$En_{98}Fs_1Wo_1$
Glass	2	59.48	0.14	26.64	0.07	1.74	0.04	1.55	4.10	3.93	0.57	98.25	–
B2-C12 (IIAB)													
Olivine	8	39.24	0.02	0.03	0.16	15.48	0.41	44.47	0.16	0.04	0.01	100.02	$Fo_{57-99.5}$
Pyroxene	11	54.71	0.04	0.36	1.04	13.29	0.62	28.04	1.06	0.11	0.01	99.27	$En_{63-83}Fs_{17-30}Wo_{0-7}$
Ca-pyroxene	1	52.35	0.21	0.98	0.83	17.31	0.93	15.03	12.78	0.39	0.00	100.81	$En_{44}Fs_{29}Wo_{27}$
Glass	8	67.13	0.21	19.87	0.02	1.30	0.04	0.16	0.91	8.54	0.08	98.25	–
B2-C13 (IIB)													
Pyroxene	7	55.74	0.15	1.58	1.58	5.52	0.34	33.03	1.88	0.03	0.01	99.86	$En_{86-90}Fs_{8-9}Wo_{2-6}$
Ca-pyroxene	2	49.53	0.83	4.28	2.08	5.24	0.81	18.53	16.12	0.06	0.00	97.47	$En_{52-60}Fs_{6-12}Wo_{34-36}$
Plagioclase	1	46.84	0.17	30.36	0.07	1.52	0.09	0.79	15.13	2.08	0.06	97.10	An_{80-84}
Glass	1	46.66	0.48	23.47	0.40	3.83	0.33	5.01	15.46	1.68	0.00	97.32	–
B2-C17 (IB)													
Olivine	3	41.29	0.01	0.04	0.15	4.74	0.17	53.21	0.15	0.02	0.00	99.77	Fo_{95-96}
Pyroxene	20	58.45	0.06	0.44	0.53	1.34	0.16	38.72	0.30	0.06	0.01	100.09	$En_{96-98}Fs_{1-3}Wo_{0-1}$
Plagioclase	1	57.89	0.55	22.51	0.38	2.67	0.21	1.71	3.81	8.78	0.70	99.21	$An_{19}Ab_{77}Or_4$
Glass	8	61.43	0.51	22.35	0.26	2.63	0.13	1.39	3.43	5.26	0.76	98.14	–
B2-C18 (IIAB)													
Olivine	1	38.09	0.02	0.00	0.12	20.93	0.50	41.17	0.13	0.01	0.00	100.96	Fo_{78}
Pyroxene	2	54.87	0.05	0.64	0.72	12.84	0.44	29.93	0.81	0.01	0.01	100.28	$En_{78-81}Fs_{18-20}Wo_{1-2}$
Ca-pyroxene	1	48.46	0.87	0.94	0.29	31.66	0.96	10.40	6.74	0.04	0.01	100.38	$En_{31}Fs_{54}Wo_{15}$
Plagioclase	4	45.35	0.05	34.01	0.01	1.14	0.02	0.24	17.75	1.28	0.02	99.86	An_{86-90}
Glass	2	53.5	0.04	28.01	0.01	1.381	0.02	0.292	7.55	7.89	0.32	99.012	–
B2-C20 (IIAB)													
Olivine	19	38.73	0.02	0.02	0.24	16.73	0.44	42.65	0.16	0.04	0.01	99.04	Fo_{76-89}
Pyroxene	6	54.76	0.06	0.37	1.23	11.72	0.59	28.10	2.24	0.14	0.01	99.21	$En_{73-94}Fs_{6-22}Wo_{0-6}$
Glass	10	72.14	0.00	16.81	0.06	2.31	0.09	0.60	0.98	6.02	0.99	100.00	–

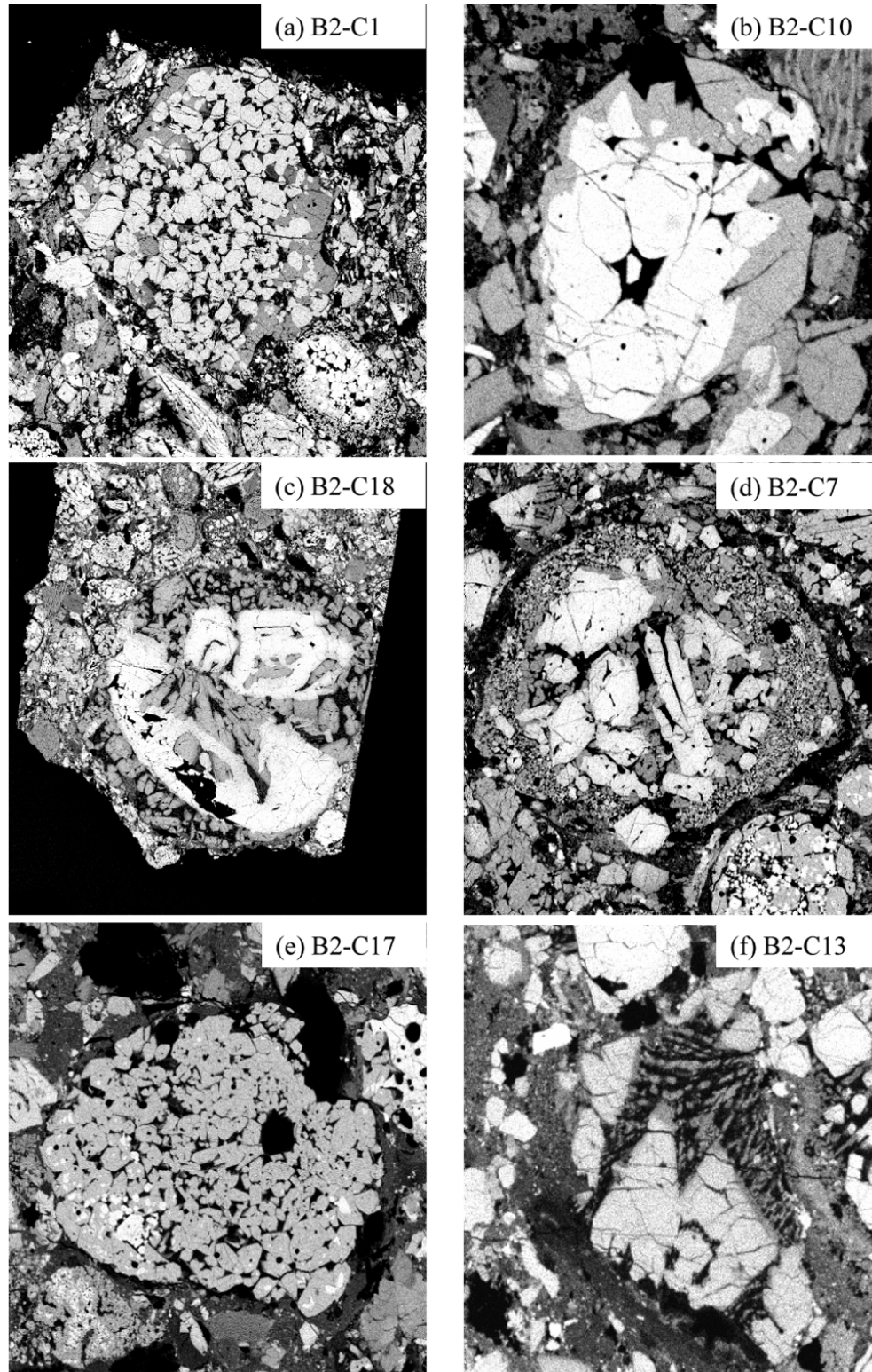*The results are mean values of the EPMA data.

FIG. 3. Magnesium x-ray maps of the chondrules studied with SIMS. Olivine is shown as light gray and pyroxene dark gray. Black areas are phases such as glass, plagioclase, metal, and sulfide. (a) B2-C1 (IIAB): Pyroxene grains are present mostly in the outer parts of the chondrule. (b) B2-C10 (IAB): The olivine grains form the core of the chondrule, while pyroxene forms the border. (c) B2-C18 (IIAB): The texture of the large olivine grain cluster (lower part) shows an outer smooth spherical shape, suggesting it is possibly the surface of a former chondrule. (d) B2-C7 (IIAB): The core is more enriched in olivine than the fine grained rim. (e) B2-C17 (IB): Pyroxene with minor poikilitically enclosed olivine that is shown clearly as bright spots. (f) B2-C13 (IIB): Euhedral pyroxene phenocrysts. Olivine is absent in the chondrule.
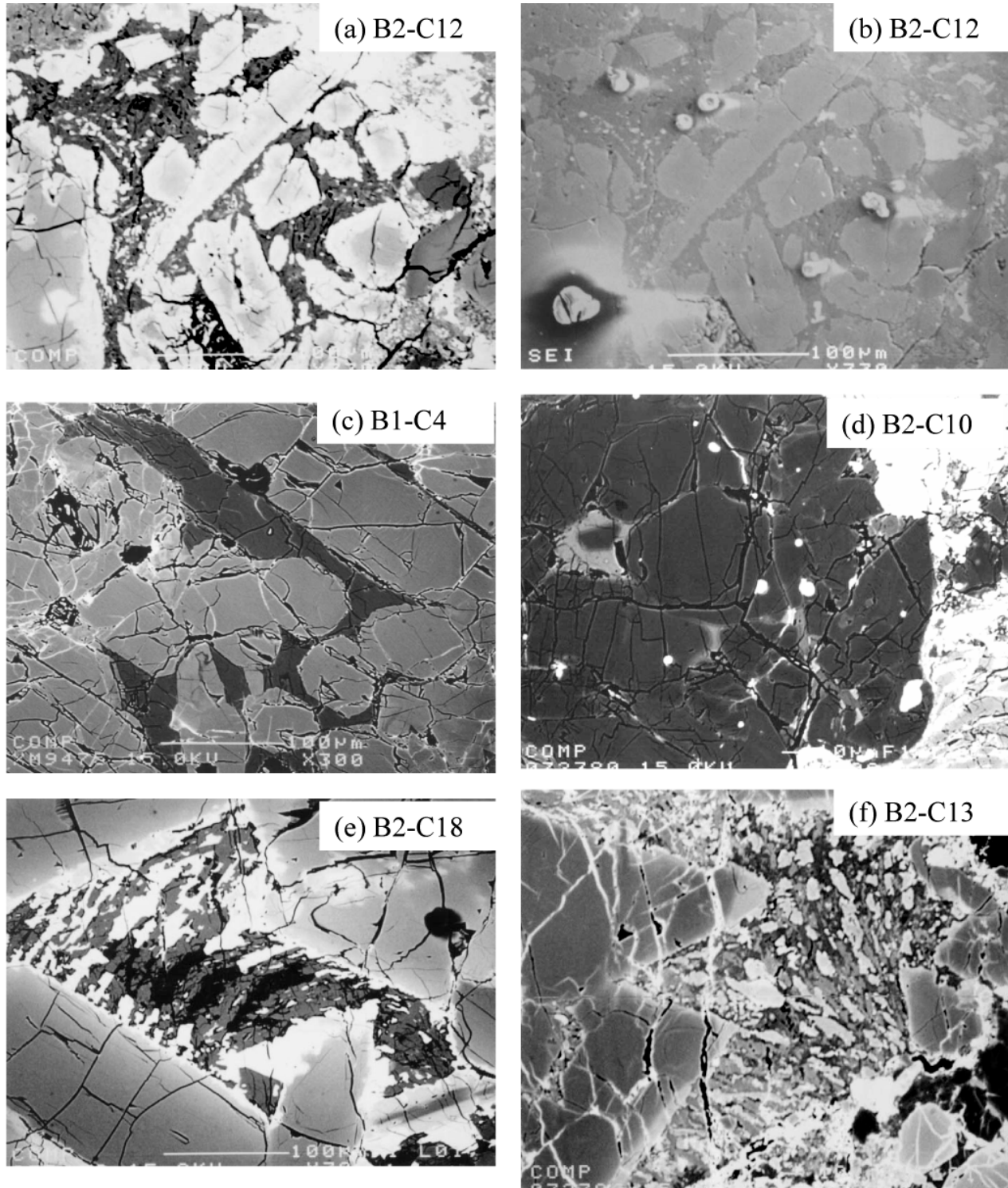
FIG. 4. Mesostases of chondrules studied with SIMS. (a) Backscattered electron (BSE) image of B2-C12 (IIAB). Zoned pyroxene phenocrysts are visible among glassy mesostasis (dark) that contains Ca-pyroxene microcrystallites. (b) Secondary electron image of the same area (a) after SIMS analyses, showing the SIMS sputtered craters right on the glassy mesostasis. One large crater at the lower left is an example of hitting mafic minerals. (c) BSE image of the central part of B1-C4 (IIAB) showing the anorthitic plagioclase (~An_{90}; dark) analyzed by SIMS. The plagioclase is filling the spaces between olivine crystals and is free of inclusions. (d) BSE image of glassy mesostasis (light gray) in B2-C10. (e) BSE image of a mesostasis area of B2-C18 (IIAB), which is surrounded by large pyroxene crystals. Fibrous crystals of plagioclase (dark gray) and Ca-pyroxene (white) are observed around glass (black). (f) Al-rich region in B2-C13 (IIB) consisting of plagioclase (gray), Ca-pyroxene (white) and glass (black), showing a radiating texture. See also Mg map for Ca-pyroxene (Fig. 3f).

these chondrules are essentially Al- and Si-rich ($SiO_2 = 60–70\%$), whereas some of the other glasses contain less silica ($SiO_2 \approx 50\%$). The Na_2O contents in plagioclase and glass are variable both within a single chondrule and among the chondrules. Since our main criterion for SIMS measurements is based on high Al/Mg in glass and plagioclase, we selected glass and plagioclase with MgO as low as possible (in most cases, from 0.1% to <1%).

The type II PP chondrule B1-C56 seem to be different from the other chondrules by its complex texture and heterogeneous olivine and plagioclase compositions (Fig. 5). The chondrule is predominantly pyroxene and is composed of grain clusters giving the illusion as if the whole object is an agglomerate of different chondrule fragments. A large pyroxene crystal is visible in the center of the chondrule and is surrounded with plagioclase. Some pyroxene grains in the chondrule are normally zoned and others show a complex intergrowth with olivine. The olivine is present in the outer parts of the pyroxene and form together a zoning-like feature (Fig. 5c). Such an olivine-pyroxene intergrowth is unusual in chondrules and, in
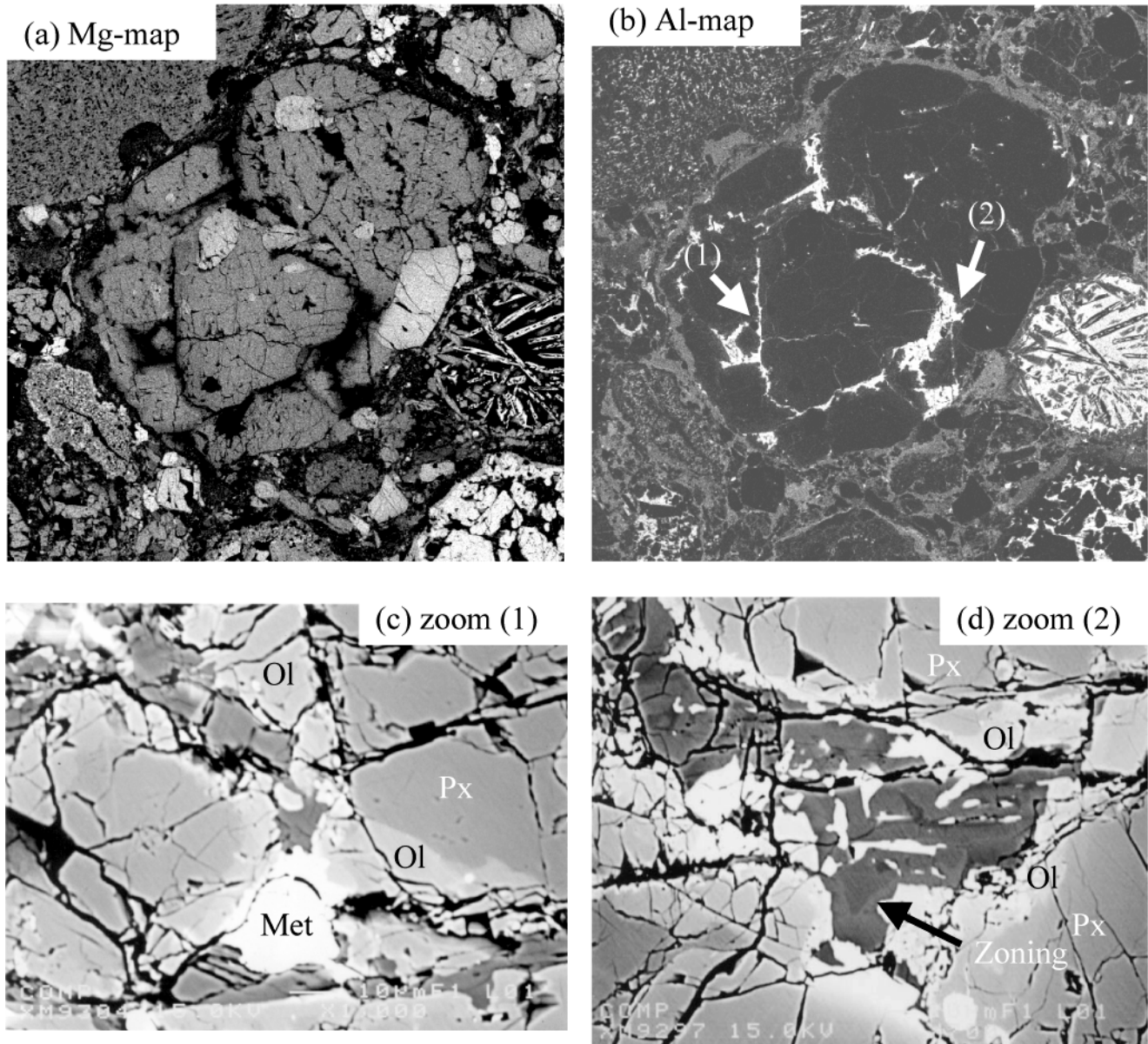

FIG. 5. SEM x-ray maps and details of B1-C56. (a) Mg map showing that the chondrule consists predominantly of pyroxene (low-Mg) with minor olivine crystals (high-Mg). A large pyroxene crystal is visible in the center of the chondrule and is totally surrounded with plagioclase. (b) Al-map showing the plagioclase around the large central crystal, and extending to the grain boundary of other pyroxenes. (c) BSE image of a plagioclase-rich region. Intergrowths of olivine (Ol) and pyroxene (Px) are observed in this chondrule, and the olivine is rimming the pyroxene forming together zoning-like features. The white region is a metal grain (Met). (d) A plagioclase-rich region showing the presence of zoned plagioclase, which can be visible by the different contrasts. Intergrown olivine with pyroxene crystals are also visible.

our knowledge, is only reported in one chondrule (see Fig. 10 in Jones, 1996), and no details are given about its origin. In B1-C56, the plagioclase is albitic and shows strong compositional zoning (An_{5-34}; Fig. 5d). It occupies the interstices of the coarse pyroxene grains and encloses Ca-pyroxene micro-crystallites. At the pyroxene grain boundaries, we also detected some FeO-rich olivine grains (Fo_{50}).

Our optical microscope observations and EPMA results reveal no secondary phases, which is consistent with the chondrules we are studying having not be subjected to significant post-crystallization alteration.

The Aluminum-26–Magnesium-26 Systematics of Bishunpur Ferromagnesian Chondrules

The results of our isotopic measurements of the Bishunpur chondrules are listed in Table 4 and plotted in isochron diagrams in Figs. 6 and 7. We made a total of 38 measurements of plagioclase and glass, ranging from 2 to 10 measurements per chondrule. Most of the analyzed areas show $^{27}Al/^{24}Mg$ ratios from 30 to 170. Five plagioclase and nine glass analyses gave values nearly or less than 30. Resolvable ^{26}Mg excesses, at the 2σ level, were obtained in most of the chondrules, with a maximum $\delta^{26}Mg$ value of 9.8‰ in two chondrules (B1-C56 and B2-C18).

We estimated the initial $^{26}Al/^{27}Al$ ratios inferred for the 11 chondrules as the slopes of Al-Mg isochron plots (Figs. 6 and 7) using the York fit program (Ludwig, 1999). In order to determine the initial $^{26}Mg/^{24}Mg$ ratios, we analyzed Mg isotopic compositions of olivine and pyroxene in three chondrules. The results show that the initial Mg isotopic ratios agree with the terrestrial standard ratio within an error of 0.2‰, which is consistent with the results reported for Semarkona ferromagnesian chondrules (Kita *et al.*, 2000). We are thus confident that the initial Mg isotopic ratios of the Bishunpur chondrules are the same as those of terrestrial standards. However, because of this assumption, admittedly, it should be mentioned that the initial $^{26}Al/^{27}Al$ ratios of chondrules without olivine and pyroxene analyses are obtained as model isochrons, unless there is a wide spread in the measured $^{27}Al/^{24}Mg$ ratios for the individual chondrules. The $^{26}Al/^{27}Al$ ratios calculated for the 11 chondrules are given in Table 5. Taken at face value, the range of the $^{26}Al/^{27}Al$ ratios (see Figs. 6 and 7) are from about $(0.35 \pm 0.48) \times 10^{-5}$ in B2-C17 to about $(2.28 \pm 0.73) \times 10^{-5}$ in B2-C1. However, given the uncertainties, B1-C18 has a barely resolved excess and B2-C7, B2-C13, and B2-C17 do not show resolved effects in a 2σ (95% confidence) level. These chondrules are best characterized as giving upper limits on the initial $^{26}Al/^{27}Al$ ratios of $<1.4 \times 10^{-5}$, $<1.2 \times 10^{-5}$, and $<0.8 \times 10^{-5}$, respectively (Table 5). Thus, the lowest resolved initial ratio becomes $(0.45 \pm 0.21) \times 10^{-5}$. These results are comparable to the values which range from 0.3×10^{-5} to 1×10^{-5} previously obtained for Semarkona and Bishunpur chondrules, (Kita *et*
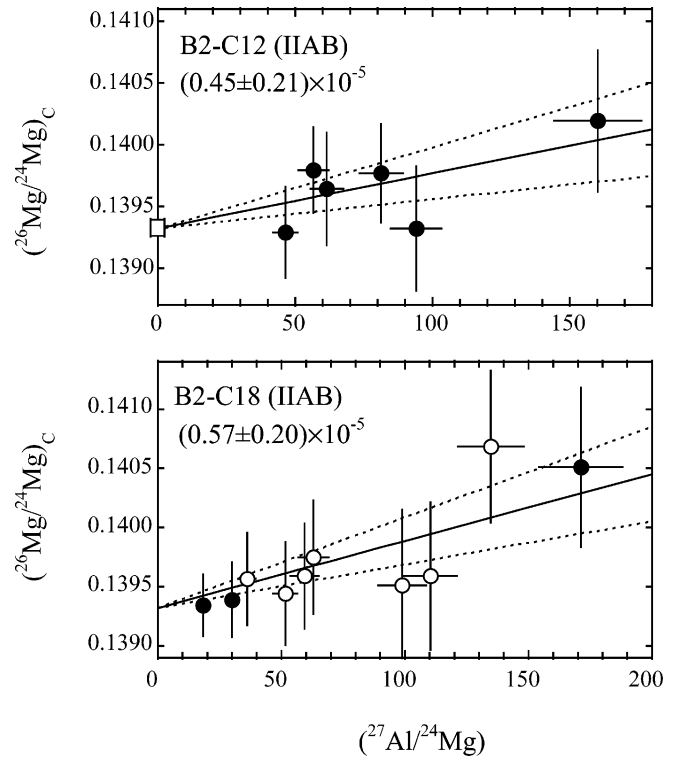
FIG. 6. ^{26}Al-^{26}Mg isochron diagrams for B2-C12 and B2-C18. Open circles are plagioclase, filled circles are glass, and an open square is olivine. The York-fitted line for each diagram is shown as a solid line and its error (2σ) limits are shown as dotted lines. The numbers in each diagram are the initial $^{26}Al/^{27}Al$ isotopic ratios obtained as the slope of the isochron.

al., 2000; McKeegan *et al.*, 2000), although extending the range towards higher $^{26}Al/^{27}Al$.

Table 5 includes the data of the albitic plagioclase bearing chondrule 1805-9 CH60 in Semarkona studied by Kita *et al.* (2000). The matrix effect of the SIMS $^{27}Al/^{24}Mg$ calibration factors resulting from plagioclase solid solution was not considered during the previous study of Semarkona chondrules. This effect reduces the initial $^{26}Al/^{27}Al$ ratio for CH60 from 0.57×10^{-5} to 0.46×10^{-5}.

Chondrules B2-C12 and B2-C18 show wide ranges in $^{27}Al/^{24}Mg$ ratios and define isochrons (Fig. 6). Most of the other chondrules show lower $^{27}Al/^{24}Mg$ ratios with marginal ^{26}Mg excesses, resulting in relatively large errors for the estimated initial $^{26}Al/^{27}Al$ ratios. In these chondrules, MgO in both glass and plagioclase is relatively high (as much as 1%) and is distributed homogeneously. The analyzed SIMS $^{27}Al/^{24}Mg$ ratios of the plagioclase and glass are mostly consistent with those obtained using EPMA. Exceptions are B1-C4, B1-C18, and B1-C56 in which the SIMS $^{27}Al/^{24}Mg$ ratios of plagioclase are much lower than the values obtained with EPMA. In the previous study of Semarkona chondrules, ion images of one chondrule showed Mg heterogeneous distribution in plagioclase grains (CH23; Kita *et al.*, 2000). In

TABLE 4. Results of the SIMS isotopic analyses of Bishunpur chondrules.

Chondrule	Analysis number	Phase	$^{27}Al/^{24}Mg$*	$(^{26}Mg/^{24}Mg)_C$[†]	$\delta^{26}Mg$ (‰)	$(^{26}Al/^{27}Al)_{initial} \times 10^{-5}$
B1-C4	#5	plagioclase	37.3	0.13962 ± 0.00041	2.1 ± 3.0	0.80 ± 1.11
	#6	plagioclase	37.6	0.14022 ± 0.00045	6.5 ± 3.2	2.39 ± 1.11
	#8	plagioclase	14.9	0.13955 ± 0.00034	1.6 ± 2.4	1.53 ± 2.26
	average					1.54 ± 0.75[‡]
B1-C18	#14	plagioclase	17.6	0.13965 ± 0.00029	2.4 ± 2.1	1.88 ± 1.67
	#5	plagioclase	31.5	0.13950 ± 0.00034	1.3 ± 2.5	0.56 ± 1.08
	average					0.95 ± 0.89[‡]
B1-C56	#1	plagioclase	47.1	0.13988 ± 0.00050	4.0 ± 3.6	1.18 ± 1.05
	#4	plagioclase	88.6	0.14069 ± 0.00074	9.8 ± 5.3	1.54 ± 0.84
	average					1.40 ± 0.65[‡]
B2-C1	#3	plagioclase	30.1	0.14007 ± 0.00031	5.4 ± 2.2	2.48 ± 1.03
	#4	plagioclase	36.7	0.14008 ± 0.00040	5.4 ± 2.8	2.07 ± 1.08
	average					2.28 ± 0.73[‡]
B2-C7	#3	glass	20.2	0.13934 ± 0.00027	0.1 ± 1.9	0.09 ± 1.34
	#2-cor	glass	21.6	0.13937 ± 0.00041	0.3 ± 2.9	0.22 ± 1.89
	#8-cor	glass	30.3	0.13968 ± 0.00041	2.6 ± 3.0	1.20 ± 1.37
	Mean					0.55 ± 0.84[‡]
B2-C10	#1bis	glass	43.6	0.13976 ± 0.00038	3.1 ± 2.7	1.00 ± 0.87
	#5	glass	44.2	0.13978 ± 0.00030	3.3 ± 2.2	1.03 ± 0.69
	MC1	olivine	= 0	0.139335 ± 0.000026		
	average					1.02 ± 0.54[‡]
B2-C12	#3	glass	94.1	0.13932 ± 0.00050	0.0 ± 3.6	0.00 ± 0.53
	#3bis	glass	160	0.14019 ± 0.00057	6.3 ± 4.1	0.55 ± 0.35
	#1	glass	81.3	0.13977 ± 0.00039	3.2 ± 2.8	0.55 ± 0.48
	#2	glass	46.5	0.13929 ± 0.00036	–0.2 ± 2.6	–0.07 ± 0.78
	#5	glass	56.7	0.13979 ± 0.00034	3.4 ± 2.4	0.84 ± 0.60
	#6	glass	61.5	0.13964 ± 0.00045	2.3 ± 3.2	0.53 ± 0.73
	MC2	olivine	= 0	0.139301 ± 0.000026		
	average					0.45 ± 0.21[‡]
B2-C13	#4	plagioclase	16.6	0.13946 ± 0.00026	1.0 ± 1.9	0.85 ± 1.58
	#1	glass	24.3	0.13960 ± 0.00028	2.0 ± 2.0	1.15 ± 1.14
	#2	glass	28.7	0.13925 ± 0.00032	–0.5 ± 2.3	–0.26 ± 1.13
	MC3	pyroxene	= 0	0.139321 ± 0.000026		
	average					0.53 ± 0.70[‡]
B2-C17	#1-cor	glass	52.6	0.13939 ± 0.00034	0.5 ± 2.5	0.14 ± 0.65
	#2-cor	glass	42.5	0.13958 ± 0.00031	1.9 ± 2.2	0.61 ± 0.74
	average					0.35 ± 0.48[‡]
B2-C18	#c1	plagioclase	51.5	0.13944 ± 0.00043	0.9 ± 3.1	0.24 ± 0.83
	#a1	plagioclase	135	0.14068 ± 0.00063	9.8 ± 4.5	1.01 ± 0.47
	#d3	plagioclase	59.4	0.13959 ± 0.00044	1.9 ± 3.1	0.46 ± 0.74
	#a7	plagioclase	63.0	0.13975 ± 0.00047	3.1 ± 3.4	0.68 ± 0.75
	#d2	plagioclase	98.8	0.13951 ± 0.00063	1.4 ± 4.5	0.20 ± 0.64
	#a2	plagioclase	110	0.13959 ± 0.00062	1.9 ± 4.4	0.24 ± 0.56
	#a6	plagioclase	36.2	0.13957 ± 0.00038	1.8 ± 2.8	0.68 ± 1.06
	#c2	glass	171	0.14051 ± 0.00066	8.5 ± 4.8	0.70 ± 0.39
	#c5-cor	glass	29.9	0.13939 ± 0.00031	0.5 ± 2.2	0.23 ± 1.03
	#1(c6)	glass	18.2	0.13934 ± 0.00025	0.2 ± 1.8	0.13 ± 1.38
	average					0.57 ± 0.20[‡]
B2-C20	#1	glass	24.5	0.13944 ± 0.00029	0.8 ± 2.1	0.48 ± 1.20
	#3-cor	glass	25.4	0.13931 ± 0.00031	0.0 ± 2.2	–0.02 ± 1.21
	#5	glass	49.1	0.13990 ± 0.00039	4.2 ± 2.8	1.19 ± 0.79
	average					0.74 ± 0.57[‡]

Errors are 2σ error (95% confidence).
*The errors of $^{27}Al/^{24}Mg$ ratios are assumed to be 10% of the analyzed values.
[†]Isotopic ratios were corrected for dead time and mass fractionation.
[‡]Data obtained using York fit.
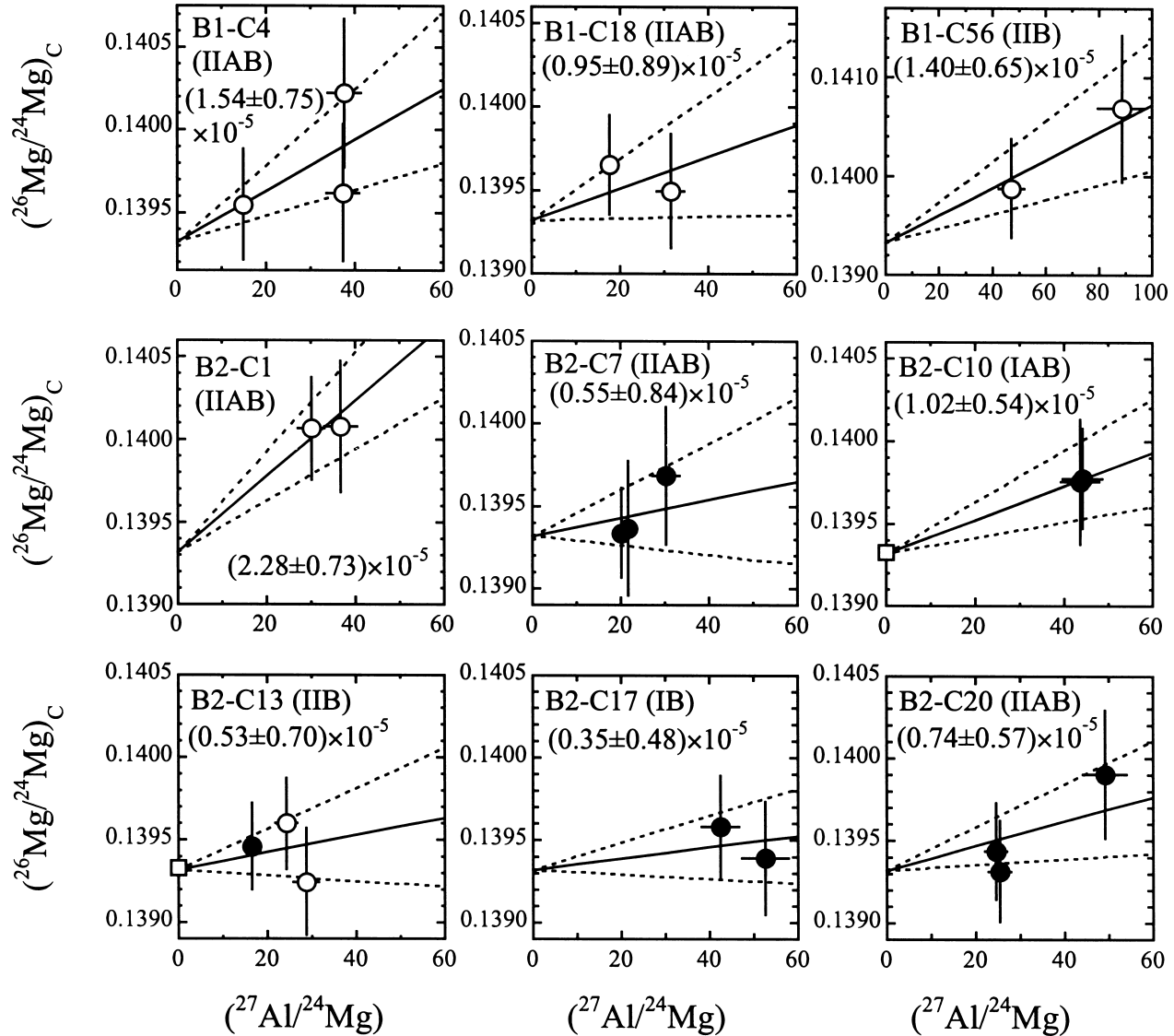
FIG. 7. ^{26}Al-^{26}Mg isochron diagrams for nine chondrules from Bishunpur. The symbols are the same as in Fig. 6. The errors of the initial ^{26}Al/^{27}Al ratios are relatively larger than those in Fig. 6, due to smaller numbers of measured points in each chondrule.

these grains, the SIMS ^{27}Al/^{24}Mg ratios are much lower than those with EPMA. In Bishunpur, the discrepancy between two analytical methods can be due to the heterogeneous distribution of Mg in plagioclase added to the fact that the measured volumes are different (*i.e.*, 2 μm for EPMA and 5–6 μm for the SIMS). With EPMA, we also tended to locate the electron beam at the center of grains having smooth surfaces, which is not applicable with SIMS. A more detailed EPMA study of the same sets of the Bishunpur chondrules (Tachibana *et al.*, unpubl. data) shows larger variations and systematically higher averages of MgO in the plagioclase. The discrepancy could also be due to the presence of tiny glass (or pyroxene) inclusions in plagioclase. In this case, the SIMS ^{27}Al/^{24}Mg calibration factors of the analyzed areas may change because those of anorthitic plagioclase (~1.3) and glass (~0.9) are significantly

different. It is possible that anorthotic plagioclase data from B1-C4 and B1-C18 shift to higher ^{27}Al/^{24}Mg ratios, resulting in a decrease of the initial ^{26}Al/^{27}Al ratios. In the case of B1-C56 with more albitic plagioclase, because the SIMS ^{27}Al/^{24}Mg calibration factor of albitic plagioclase is similar to that of glass, the presence of glass inclusions may not change the initial ^{26}Al/^{27}Al ratio of the chondrule listed in Table 4.

If we adopt the ^{26}Al-^{26}Mg system as a chronometer by assuming a homogeneous distribution of ^{26}Al in the early solar system, the deviation of the ^{26}Al/^{27}Al ratio in a given chondrule from CAIs will correspond to an age relative to CAIs. Using the canonical peak value of 4.5×10^{-5} from type B1 CAIs (MacPherson *et al.*, 1995), our ^{26}Al/^{27}Al ratios for the Bishunpur chondrules, ranging from $(2.28 \pm 0.73) \times 10^{-5}$ to $(0.45 \pm 0.21) \times 10^{-5}$, correspond to ages relative to CAIs

TABLE 5. Initial $^{26}Al/^{27}Al$ ratios of Bishunpur chondrules and formation ages relative to CAIs.*

Chondrule	Px (%)	$(^{26}Al/^{27}Al) \times 10^{-5}$	ΔT_{CAI} (Ma)
B1-C4	22	1.54 ± 0.75	$1.13\,^{-0.42}_{+0.70}$
B2-C1	24	2.28 ± 0.73	$0.72\,^{-0.16}_{+0.18}$
B2-C10	26	1.02 ± 0.54	$1.56\,^{-0.45}_{+0.79}$
B2-C20	30	0.74 ± 0.57	$1.90\,^{-0.60}_{+1.53}$
B1-C18	43	0.95 ± 0.89	$1.64\,^{-0.70}_{+2.89}$
B2-C18	46	0.57 ± 0.20	$2.18\,^{-0.32}_{+0.46}$
B2-C7	52	<1.39	>1.24
B2-C12	56	0.45 ± 0.21	$2.43\,^{-0.41}_{+0.67}$
B1-C56	87	1.40 ± 0.65	$1.23\,^{-0.40}_{+0.66}$
B2-C17	95	<0.83	>1.78
B2-C13	100	<1.23	>1.37
Semarkona†			
1805-9 CH60	83	0. 46 ± 0.21	$2.41\,^{-0.40}_{+0.65}$

*The ages of chondrules are calculated relative to the average ages of CAIs, assuming an initial $(^{26}Al/^{27}Al)$ ratio of 4.5×10^{-5} for CAIs (MacPherson *et al.*, 1995).
†Recalculated value from Kita *et al.* (2000); see text for details.

between 0.7 ± 0.2 Ma and $2.4\,^{-0.4}_{+0.7}$ Ma (Table 5). As the initial $^{26}Al/^{27}Al$ ratios of some chondrules in this study are higher than those previously found in Semarkona and Bishunpur chondrules (Kita *et al.*, 2000; McKeegan *et al.*, 2000), the oldest formation time of chondrules becomes <1 Ma after CAI formation. Considering the maximum required time interval comes from the extremes of the error envelopes for the initial ratios (*i.e.*, 2.28–0.73 = 1.54×10^{-5} to 0.45 + 0.21 = 0.66×10^{-5}), the demonstrated spread between chondrules will correspond to a time span of ~1 Ma between the earliest and latest formed chondrules.

Age-Composition Correlation in Bishunpur Chondrules

In an attempt to investigate the possibility of a relationship between the ages of chondrules and their chemical compositions, we examined the inferred initial $^{26}Al/^{27}Al$ (and the corresponding relative ages) as a function of the proportion of pyroxene (defined as $px = $ [pyroxene]/[olivine + pyroxene]) in the chondrules. Figure 8 shows that the $^{26}Al/^{27}Al$ ratio increases (or age decreases) with decreasing proportion of pyroxene, suggesting that the olivine-rich chondrules are older than the pyroxene-rich chondrules. In Fig. 8, we also plotted data from Semarkona chondrules reported by Kita *et al.* (2000) using the new value from this paper and from a Semarkona clast chondrule (1805-CC1) by Hutcheon and Hutchison (1989). The Semarkona data also lie on the same trend suggesting the correlation is valid. As shown in the diagram, there is no systematic difference between type I and type II chondrules. The only chondrule scattering from the correlation is B1-C56, which shows a relatively higher $^{26}Al/^{27}Al$ ratio. As we mentioned earlier, this chondrule has a complex texture, though it is not a sufficient reason to single it out. If the chondrule has been disturbed by secondary processes, one might expect it to show an unusually low $^{26}Al/^{27}Al$ ratio. It is uncertain that the calculated ^{26}Al ages (or the logarithm of the $^{26}Al/^{27}Al$ ratio) linearly correlate with *px*. Nonetheless, among the whole range of the data set the Fig. 8 indicates that the olivine-rich chondrules have relatively high $^{26}Al/^{27}Al$ ratios.

DISCUSSION

Total Span of Chondrule-Forming Events

With data available to date, we can not clearly prove or disprove the question of whether ^{26}Al was distributed homogeneously in the early solar system, which is the basis of applying the ^{26}Al-^{26}Mg chronometer (*e.g.*, MacPherson *et al.*, 1995; Kita *et al.*, 2000). However, arguments in favor of the age interpretation are persuasive as discussed in detail by Huss *et al.* (2001) (see also the review paper of MacPherson *et al.*, 1995). In fact, the initial $^{26}Al/^{27}Al$ ratios of chondrules obtained from unmetamorphosed carbonaceous chondrites (Hutcheon *et al.*, 2000; Srinivasan *et al.*, 2000a,b) show the same range as those from Semarkona and Bishunpur, despite their different oxygen isotope compositions. This suggests that, regardless of the location, ^{26}Al was distributed homogeneously in the solar nebula and the chondrule formation events may have occurred at the same time. In our previous work on Semarkona chondrules (Kita *et al.*, 2000), the significant variation in the initial $^{26}Al/^{27}Al$ ratios was not considered. As discussed above, the initial $^{26}Al/^{27}Al$ ratios of Bishunpur chondrules range from $(0.45 \pm 0.21) \times 10^{-5}$ to $(2.28 \pm 0.73) \times 10^{-5}$, demonstrating a total time span of at least 1 Ma, assuming a homogeneous distribution of the ^{26}Al. The large variation of the initial $^{26}Al/^{27}Al$ ratios (by a factor of 5) among chondrules is in contrast to the prominent variation among CAIs $((4–5) \times 10^{-5})$. Even though some of the data show relatively large errors, the whole data set of Bishunpur and Semarkona chondrules is consistent with chondrule formation events taking place over more than 1 Ma. This is much longer than the timescale inferred for the active nebula (~0.1 Ma), and suggests that chondrule
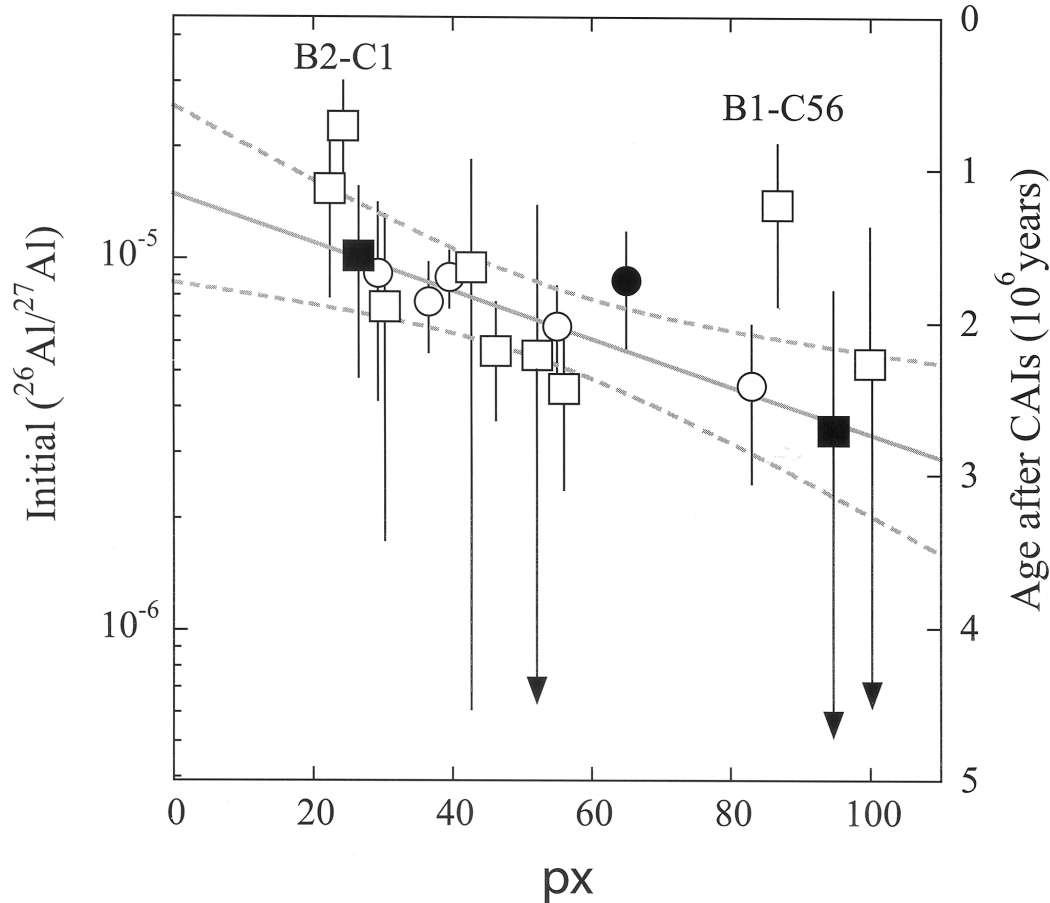
FIG. 8. Correlation between the [26]Al ages and the proportion of pyroxene among ferromagnesian chondrules in Bishunpur (squares) and Semarkona (circles). Semarkona data are after Hutcheon and Hutchison (1989) and Kita *et al.* (2000). Type I (FeO-poor) chondrules are shown as filled symbols and type II (FeO-rich) chondrules as open symbols. The gray solid line and dashed lines are the best-fit line and its error limits (95% confidence level), respectively, using the least-square method (Tachibana *et al.*, 2001). The error of the proportion of pyroxene is not considered in the figure. The data suggest that olivine-rich chondrules formed earlier than pyroxene-rich chondrules.

formation may not be explained by the protostar embedded stage of the X-wind model (Shu *et al.*, 1996), if the production of the [26]Al is neglected.

If the [26]Al was locally produced by the X-wind model, the observed variation in the initial Al isotopic ratios will not correspond to a time difference. However, as discussed by Huss *et al.* (2001), the local production of [26]Al in CAIs and chondrules by irradiation credited by the X-wind model (Shu *et al.*, 1996) has a serious difficulty in producing [26]Al without overproducing other radionuclides, such as [10]Be, [41]Ca, and [53]Mn. For this reason, we favor the age interpretation and consider in the following discussion that the [26]Al-[26]Mg system is a chronometer.

Olivine-Rich Chondrules Appear to be Older than Pyroxene-Rich Chondrules

A relationship between CAIs and chondrules has always been discussed in terms of elemental fractionation among precursors and/or constitutive minerals formed during chondrule formation (McSween, 1977; Bischoff and Keil, 1984; MacPherson and Huss, 2000). MacPherson and Huss (2000) suggested a sequential chemical evolution from CAIs to Al-rich chondrules and type I chondrules. Also, several authors have advocated the possibility of the formation of type I chondrules from more oxidized and volatile-rich type II chondrules (*e.g.*, Sears *et al.*, 1996). However, due to the lack of systematical chronological data for ferromagnesian chondrules, none of these studies have been able to discuss such issues in terms of a timescale. The diagram in Fig. 8 is the first report of a correlation between age and composition of chondrules. The *px* of chondrules increases with time. Tachibana *et al.* (2001) have recently measured the bulk compositions of the same chondrules we studied, and found a similar correlation of decreasing Si/Mg and volatile-elements/Mg ratios with age. These results are consistent with the correlation in Fig. 8 suggesting that olivine-rich chondrules are older than pyroxene-rich ones. Detailed compositional data for the chondrules discussed here will be reported in an upcoming paper.

At present, we do not have a satisfactory explanation for the correlation. However, we suggest that the mechanism responsible for the observed correlation is probably the key to understanding the chondrule formation process(es). We now discuss this issue by considering nebular condensation and elemental fractionation

Two possible mechanisms that might account for the observations:

(1) Chondrule Formation in a Cooling Nebular Gas– The canonical nebular model predicts that pyroxene condenses subsequent to olivine (Grossman, 1972). This is in concordance with the correlation in Fig. 8. Indeed, if chondrules are formed by any transient events in a nebula that is continuously cooling and changing in composition, the bulk compositions and the nature of the constituent minerals of the chondrules should reflect those of their precursor "nebular" materials. The total time span of our chondrule ages (~1 Ma) can thus be interpreted as a cooling timescale of the nebula, in which the chemical compositions of the chondrule precursors change from olivine-rich to pyroxene-rich.

While this interpretation seems to be reasonable from the point of view of chemistry, it is not compatible with kinetic considerations from some recent astronomical observations. Both forsterite and enstatite condense at high temperature (~1300 K), and the condensation temperature of enstatite is only slightly lower than that of forsterite by 100 K (Grossman, 1972). The 1 Ma chondrule formation period estimated here appears to be too long for cooling through 100 K. Theoretical models can produce cooling rates of 100 K/Ma by adjusting parameters, such as kinematic velocity, mass accretion rate and others. However, observations of young stars show that the timescale of classical T Tauri stars (high-temperature phase) is ~1 Ma (Hartmann, 1996), and thus the temperature would decrease by several hundred degrees during 1 Ma. This indicates that the cooling rate of ~100 K/1 Ma is too low.

(2) Volatile Loss During Chondrule Formation–The transition from olivine-rich to pyroxene-rich chondrules could be the result of elemental fractionation either during or prior to chondrule formation from already fractionated precursors. In the latter case, compositional differences between the precursors would reflect either the difference in time at which they were separated from the system, or the difference in place where they were formed (or perhaps even the difference in temperature they experienced). Alternatively, considering that an olivine-rich composition is less volatile than a pyroxene-rich composition, it is likely that elemental fractionation between Mg and Si might have occurred during the chondrule formation process by evaporation processes. It is possible that Si evaporated from chondrules more than Mg during chondrule formation at high temperature to form olivine-rich compositions. Silicon would then be added to the precursors of the next generation of chondrules. Hence, younger chondrules would become more enriched in pyroxene. Nagahara *et al.* (1999) observed enrichments of Si and Na in chondrule glass near the chondrule surface and interpreted this as due to the re-condensation of evaporated Si and other volatiles during chondrule formation.

If a volatility-controlled process was involved, we may expect a correlation between ages of chondrules and their volatile element contents, such as Na and Fe. As described above, we did not find any systematic difference between type I and type II chondrules; in other words there is no correlation between age and FeO contents of chondrules. However, other volatile elements, such as Na and Mn, do seem to correlate with age (Tachibana *et al.*, 2001). Jones (1994) reported that there are positive correlations between bulk Na, Mn, and Cr contents and SiO_2% among type I chondrules. Nyquist *et al.* (2001) found that Mn/Cr and Mn/Sc ratios of radial pyroxene chondrules are higher than those of olivine-rich chondrules. Considering that Mn is more volatile than Cr and Sc, this tendency is a good indication that the pyroxene-rich chondrules are more enriched in volatiles than the olivine–rich ones. For these reasons, it is conceivable that Si and other volatile elements were lost from olivine-rich chondrules and added to the precursors of later forming chondrules enriched in pyroxene. The relationship between Si and Fe contents is complicated because Fe could be present as metal in type I chondrules that could have been expelled from, or captured in, molten chondrules as metal droplets.

CONCLUSIONS

The ^{26}Al-^{26}Mg isotopic systematics of 11 ferromagnesian chondrules from the highly unequilibrated ordinary chondrite Bishunpur were determined. Excesses in ^{26}Mg were detected in many glasses and plagioclase in the chondrules. The initial $^{26}Al/^{27}Al$ ratios inferred for the chondrules range from $(2.28 \pm 0.73) \times 10^{-5}$ to $(0.45 \pm 0.21) \times 10^{-5}$. Assuming a homogeneous distribution of Al isotopes in the early solar system, the ages of the chondrules are found to range from 0.7 ± 0.2 Ma to $2.4^{-0.4}_{+0.7}$ Ma after CAI formation. A total time span of chondrule formation of ~1 Ma is too long to form chondrules by the embedded stage of the X-wind model, which lasted for only ~0.1 Ma.

The Bishunpur chondrules analyzed show a wide range of olivine and pyroxene contents and a correlation is found between the initial $^{26}Al/^{27}Al$ ratio of individual chondrules and the proportion of olivine to pyroxene. The correlation suggests that olivine-rich chondrules formed earlier than pyroxene-rich chondrules. A similar trend is observed in Semarkona chondrules (data from Kita *et al.*, 2000), thus supporting the correlation. The range of the initial $^{26}Al/^{27}Al$ ratios inferred for the Bishunpur chondrules is wider than that for the Semarkona chondrules (Kita *et al.*, 2000). This may be because a wider compositional range was examined in Bishunpur. At present we do not have a clear explanation of the observed correlation. One possible mechanism is the elemental fractionation of Si by evaporative loss from older

chondrules (olivine-rich) followed by its later addition to the precursors of younger ones (pyroxene-rich). Further studies combining chondrule chronology with chemistry may improve our understanding of the process of chondrule formation and its relationship to nebular evolution.

Editorial handling: K. D. McKeegan

REFERENCES

BISCHOFF A. AND KEIL K. (1984) Al-rich objects in ordinary chondrites: Related origin of carbonaceous and ordinary chondrites and their constituents. *Geochim. Cosmochim. Acta* **48**, 693–709.

GOODING J. H. AND KEIL K. (1981) Relative abundances of chondrule primary textural types in ordinary chondrites and their bearing on conditions of chondrule formation. *Meteoritics* **16**, 1–17.

GROSSMAN L. (1972) Condensation in the primitive solar nebula. *Geochim. Cosmochim. Acta* **36**, 597–619.

HARTMANN L. (1996) Astronomical observations of phenomena in protostellar Disk. In *Chondrules and the Protoplanetary Disk* (eds. R. H. Hewins, R. H. Jones and E. R. D. Scott), pp. 13–20. Cambridge University Press, Cambridge, U.K.

HUSS G. R., MACPHERSON G. J., WASSERBURG G. J., RUSSELL S. S. AND SRINIVASAN G. (2001) Aluminum-26 in calcium-aluminum-rich inclusions and chondrules from unequilibrated ordinary chondrites. *Meteorit. Planet. Sci.* **36**, 975–997.

HUTCHEON I. D. AND HUTCHISON R. (1989) Evidence from Semarkona ordinary chondrite for ^{26}Al heating small planets. *Nature* **337**, 238–241.

HUTCHEON I. D. AND JONES R. H. (1995) The ^{26}Al-^{26}Mg record of chondrules: Clues to nebular chronology (abstract). *Lunar Planet. Sci.* **26**, 647–648.

HUTCHEON I. D., KROT A. N. AND ULYANOV A. A. (2000) ^{26}Al in anorthite-rich chondrules in primitive carbonaceous chondrites: Evidence chondrules postdate CAI (abstract). *Lunar Planet. Sci.* **31**, #1869, Lunar and Planetary Institute, Houston, Texas, USA (CD-ROM).

IMAI N., TERASHIMA S., ITOH S. AND ANDO A. (1995) 1994 compilation of analytical data for minor and trace elements in seventeen GSJ geochemical reference samples, "Igneous rock series". *Geostandards Newsletter* **19**, 135–213.

JOCHUM K. P. *ET AL.* (2000) The preparation and preliminary characterisation of eight geological MPI-DING reference glasses for *in situ* microanalysis. *Geostandards Newsletter* **24**, 87–133.

JONES R. H. (1994) Petrology of FeO-poor, porphyritic pyroxene chondrules in the Semarkona chondrite. *Geochim. Cosmochim. Acta* **58**, 5325–5340.

JONES R. H. (1996) FeO-rich, porphyritic pyroxene chondrules in unequilibrated ordinary chondrites. *Geochim. Cosmochim. Acta* **60**, 3115–3138.

KITA N. T., NAGAHARA H., TOGASHI S. AND MORISHITA Y. (2000) A short duration of chondrule formation in the solar nebula: Evidence from ^{26}Al in Semarkona ferromagnesian chondrules. *Geochim. Cosmochim. Acta* **64**, 3913–3922.

LUDWIG K. R. (1999) *Using Isoplot/Ex, Version 2.01: A Geochronological Toolkit for Microsoft Excel.* Berkeley Geochronology Center Special Publication, **No. 1a**, Berkeley, California, USA. 47 pp.

MACPHERSON G. J. AND HUSS G. R. (2000) Convergent evolution of CAIs and chondrules: Evidence from bulk composition and a cosmochemical phase diagram (abstract). *Lunar Planet. Sci.* **31**, #1796, Lunar and Planetary Institute, Houston, Texas, USA (CD-ROM).

MACPHERSON G. J., DAVIS A. M. AND ZINNER E. K. (1995) The distribution of ^{26}Al in the early solar system—A reappraisal. *Meteoritics* **30**, 365–386.

MCKEEGAN K. D., GREENWOOD J. P., LESHIN L. A. AND COSARINSKY M. (2000) Abundance of ^{26}Al in ferromagnesian chondrules of unequilibrated ordinary chondrites (abstract). *Lunar Planet. Sci.* **31**, #2009, Lunar and Planetary Institute, Houston, Texas, USA (CD-ROM).

MCSWEEN H. Y., JR. (1977) Chemical and petrographical constraints on the origin of chondrules and inclusions in carbonaceous chondrites. *Geochim. Cosmochim. Acta* **41**, 1843–1860.

MOSTEFAOUI S., PERRON C., ZINNER E. AND SAGON G. (2000) Metal-associated carbon in primitive chondrites: Structure, isotopic composition, and origin. *Geochim. Cosmochim. Acta* **64**, 1945–1964.

NAGAHARA H., KITA N. T., OZAWA K. AND MORISHITA Y. (1999) Condensation during chondrule formation: Elemental and Mg isotopic evidence (abstract). *Lunar Planet. Sci.* **30**, #1342, Lunar and Planetary Institute, Houston, Texas, USA (CD-ROM).

NYQUIST L. E., LINDSTROM D., MITTLEFEHLDT D., SHIH C-Y., WIESMANN H., WENTWORTH S. AND MARTINEZ R. (2001) Manganese-chromium formation intervals for chondrules from the Bishunpur and Chainpur meteorites. *Meteorit. Planet. Sci.* **36**, 911–938.

RAMBALDI E. R. AND WASSON J. T. (1981) Metal and associated phases in Bishunpur, a highly unequilibrated ordinary chondrite. *Geochim. Cosmochim. Acta* **45**, 1001–1015.

RUSSELL S. S., SRINIVASAN G., HUSS G. R., WASSERBURG G. J. AND MACPHERSON G. J. (1996) Evidence for widespread ^{26}Al in the solar nebula and constraints for nebula time scales. *Science* **273**, 757–762.

SEARS D. W. G., HUANG S. AND BENOIT P. H. (1996) Open-system behaviour during chondrule formation. In *Chondrules and the Protoplanetary Disk* (eds. R. H. Hewins, R. H. Jones and E. R. D. Scott), pp. 221–231. Cambridge University Press, Cambridge, U.K.

SHU F. H., SHANG H. AND LEE T. (1996) Toward an astrophysical theory of chondrites. *Science* **271**, 1545–1552.

SRINIVASAN G., HUSS G. R. AND WASSERBURG G. J. (2000a) A petrographic, chemical, and isotopic study of calcium-aluminum-rich inclusions and aluminum-rich chondrules from the Axtell (CV3) chondrite. *Meteorit. Planet. Sci.* **35**, 1333–1354.

SRINIVASAN G., KROT A. N. AND ULYANOV A. A. (2000b) Aluminum-magnesium systematics in anorthite-rich chondrules and calcium-aluminum-rich inclusions from reduced CV chondrite Efremovka (abstract). *Meteorit. Planet. Sci.* **35 (Suppl.)**, A151–A152.

TACHIBANA S., KITA N. T., NAGAHARA H. AND MOSTEFAOUI S. (2001) Correlation between relative ages and bulk compositions of ferromagnesian chondrules from highly unequilibrated chondrules (abstract). *Meteorit. Planet. Sci.* **36 (Suppl.)**, A202.